Article

In Situ Tensile Testing under High Speed Optical Recording to Determine Hierarchical Damage Kinetics in Polymer Layers of Flax Fibre Elements

Emmanuelle Richely [1], Johnny Beaugrand [1,*], Michel Coret [2], Christophe Binetruy [2], Pierre Ouagne [3], Alain Bourmaud [4] and Sofiane Guessasma [1,*]

[1] INRAE, Research Unit BIA UR1268, Rue Geraudiere, F-44316 Nantes, France
[2] Nantes Université, École Centrale de Nantes, CNRS, GeM,UMR 6183, Lab Therm & Energie Nantes, LTeN,UMR 6, F-44000 Nantes, France
[3] Université de Toulouse, INP-ENIT, Laboratoire Génie de Production (LGP), Tarbes, France;
[4] Univ. Bretagne Sud, UMR CNRS 6027, IRDL, F-56100 Lorient, France
* Correspondence: authors: johnny.beaugrand@inrae.fr; Sofiane.guessasma@inrae.fr

Abstract: This study aims at better understanding the damage and fracture kinetics in flax fibres elements at both the unitary and bundle scales using an experimental setup allowing optical observation at high recording rate in the course of tensile loading. Defects issues from flax unitary fibre extraction are quantitated using polarized light microscopy. Tensile loading is conducted according to a particular setup adapted to fibres of 10 to 20 µm in diameter and 10 mm in length. Optical recording using high speed camera is performed during loading up to the failure at acquisition speed ranging from 108,000 to 270,000 frames per second. Crack initiation in polymer layers of fibre elements, propagation as well as damage mechanisms are captured. The results show different failure scenarios depending on the fibre element nature. In particular, fractured fibres underline either a fully transverse failure propagation or a combination of transverse and longitudinal cracking with different balances. Image recordings with high time resolution down to 3.7 µs suggest unstable system and transverse crack speed higher than 4 m/s and a slower propagation for longitudinal crack deviation.

Keywords: flax fibre; tensile testing; crack propagation; fractography; high-speed optical imaging; microstructure; *in-situ* tensile testing

1. Introduction

Flax is currently viewed as one of the most promising plant fibre to replace synthetic materials such as glass in composite industry [1]. Thanks to large specific mechanical performance of flax fibres, light and sustainable technical parts can challenge traditional counterparts [2]. Flax fibers are derived from the stems of the flax plant. It has a hierarchical structure with a large complexity composed of primary and secondary cell walls. The primary wall is the outermost layer of the fibre. It is composed of cellulose microfibrils, hemicellulose, and pectin. The primary cell wall is at the origin of the fibre flexibility and ability to bend and twist. The secondary cell wall is located beneath the primary cell wall and is composed mainly of cellulose microfibrils and amorphous polymers like hemicellulose and lignin [3]. The secondary cell wall is responsible for the fibre strength and stiffness, making it resistant to breaking and tearing. As it is the case for plant fibres, flax usage is threatened by the property variability which is triggered by its genuine phenotype and extraction processes [4]. The effect of this variability on the mechanical performance is amplified by the global warming [5]. Thus, the understanding of the link between the structure and the performance of plant fibres element such as flax is important to quantify the effect of variability and adopt strategies to attenuate its effect within the context of large-scale manufacturing. Several ways exist to act in that regards with both leverages at fibre genetics and extraction parameters. For instance, generation of new porosity and

 doi:10.20944/preprints202305.2090.v1

disruption in MFA (microfibril angle) have been reported due to plant fibre extraction machines [6-10] [11]. The damage caused by the mechanical extraction influences the mechanical performance of genuine fibres elements as well as the fibre-based composites [9]. This damage involves complex deformation mechanisms due to the interaction with the core structure of the fibre such as the lumen and the roughness [12-14]. These mechanisms promote stress localisation phenomena, which are difficult to capture if *in-situ* testing or numerical models that use exact fibre elements ultrastructure are not considered. These defects gain in role at the composite level through the intrinsic fibre properties or the interfacial properties. Both result in various failure scenarios depending on the compatibility and the fibre surface treatments considered to improve the load transfer between the matrix and the fibre [15] [16, 17] [18, 19]. When it is not possible to use elementary or also called unitary fibres as reinforcement, bundles potentially close the gap. However, bundles add more complexity because of the role of the middle lamella [20, 21]. Here, at least three main scales need to be investigated to anticipate the composite performance, namely unitary fibre, bundle and composite microstructure.

Many attempts have been made to understand the unitary fibre and bundle scale on the failure properties of flax [22]. By means of scanning electron microscopy and acoustic emission, Romhany et al. [22] showed that flax bundle exhibits a combination of axial splitting of the unitary fibres and radial cracking. Barbulée et al. [23] reported a frictional behaviour of unitary fibres under tension within the flax bundle and delamination process, which compete with a transverse fibre rupture. Ahmed et al. [24] compared the effect of the unitary fibre and bundle scales on the mechanical behaviour of flax using scanning electron microscopy. A sequential rupture scenario has been suggested, which encompasses bundle rotation, unitary fibres segregation and ultimate failure. Fuentes et al. [14] reported deformation mechanisms of hemp bundle for by using digital image correlation. The authors showed that interfacial behaviour explains the ultimate performance of bundles as a significant shearing is witnessed for weak bundles and transverse rupture of unitary fibres for strong ones.

In terms of defect role in rupture properties, Mott et al. [25] reported tensile results in wood fibres conducted under SEM observation where defects acted as preferred sites for failure. Also, Baley [26] demonstrated, through SEM observations, the crack initiation from kink bands in flax fibres. Aslan et al. [27] demonstrated the link between variability in properties and the defect distribution in unitary flax fibres. In particular, optical microscopy and SEM results showed a fracturing behaviour originating from both internal and surface defects.

Despite great effort dedicated to the quantification of the result of rupture behaviour in unitary natural fibres and bundles using either *post mortem* or SEM in-situ observations, the kinetics and ranking of deformation mechanisms cannot be easily understood. On top of that, the role of defects in defining the rupture scenarios are not thoroughly described. High speed optical recording has been envisaged as a way to capture the rupture events in natural fibre elements and related composites [28, 29]. These observations highlight increasing complexity in damage initiation and growth depending on the scale. Transverse, longitudinal cracking and bridging phenomena are all reported as competing deformation mechanisms where defects are identified as potential sites for crack initiation. Because of the multiple surface defects combined with a rapid crack propagation, monitoring failure is challenging because of the difficulty to maintain a high frame rate while observing a large region of interest. Some attempts were made to address this difficulty by performing notches on the fibres prior to testing to obtain a more localised rupture [28].

With most recent progresses in terms of recording velocity by high speed cameras, it is now possible to decipher the mechanisms involved during the failure in flax fibres without guiding the crack initiation. This study aims at providing a clear view of the deformation mechanisms in flax at both the unitary fibre and bundle scales with focuses on the failure scenarios, crack initiation and propagation paths.

This study addresses, firstly, the topography and the chemical composition of flax fibres elements as well as the quantification of the defect density and extent from polarized light microscopy. Secondly, optical imaging at high acquisition rates is conducted during tensile loading

 doi:10.20944/preprints202305.2090.v1

to explore the damage growth in flax fibre elements. The damage mechanisms are discussed according to various cracking models.

2. Experimental layout

2.1. Materials

Bolchoï variety is selected as a high-fibre yield textile flax fibre for testing. Dew-retted flax stems were provided by Groupe Depestele / Teillage Vandecandelaère. These were cultivated in France and dew-retted in the field in 2017. After harvesting, the plants were stored, scutched and hackled. The fibre bundles obtained were then intentionally damaged by crushing between rollers on a pilot scutching line (ENI-Tarbes). Therefore, unitary fibres extracted from scutched bundles with contrasted defect density were extracted manually depending on the location, *i.e.* close or in-between the marks left by the rollers.

2.2. Biochemical composition

For all biochemical analysis, a first step of homogenization was performed by cryogrinding (SPEX 6700 freezer Mill) into a powder approximately 2g of raw flax bundles from the middle part of the scutched technical flax fibres (about 60 cm long) from each batch. The results given are the mean values expressed as the percentage of dry matter.

- Monosaccharides:

The flax powdered samples (approximately 5mg per trial) were subjected to a pre-hydrolysis in 12M H_2SO_4 (Sigma Aldrich) during 2 hours at 25°C. An additional hydrolysis step in 1.5M H_2SO_4 was performed during 2 hours at 100°C after addition of inositol used as an internal standard. The alditol acetate derivatives of the neutral sugars [30] were analysed by gas phase chromatography (Perkin Elmer, Clarus 580, Shelton, CT, USA) equipped with an DB 225 capillary column (J&W Scientific, Folsorn, CA, USA) at 205 °C, with H_2 as the carrier gas and a flame ionisation detector. Standard monosaccharide solutions of known concentrations were used as calibration. The galacturonic and glucuronic acids were merged as uronic acids and determined by the m-hydroxybiphenyl method [31], a colorimetric quantification. Three independent assays were performed for each analysis.

- Lignin:

The lignin content was quantified by spectrophotometry following the acetyl-bromid method [32]. Three independent assays were performed for each fibre batch and the chemicals were laboratory grade from Sigma Aldrich.

- Proteins:

The protein content was estimated by the C/N method of Dumas, which enable to measure the nitrogen, carbon and sulphur content by fast and complete combustion of the sample using an elemental analyser (VarioMicro, Elementar). The protein content is derived from the nitrogen content using a conversion factor of 6.25, following the general case. The determination of conversion factors is still a moot point [33] and two independent trials were performed.

2.3. Sample preparation

Flax fibres elements, as unitary or bundles, were glued on cardboard frames prepared by laser cut and adapted for an optimal control of the fibre alignment on the tensile bench. Unitary fibres were extracted manually from bundles. All samples used in this study were scanned by optical microscopy prior to tensile testing in order to characterize their morphology and defect distribution. Optical images were obtained using a microscope (Leitz DMRB, Leica Microsystems, Nanterre, France) equipped with a Hamamatsu digital camera (C11440 ORCA-Flash4.0 LT). Large image scanning was performed thanks to a motorized stage (Marzhauser), allowing a scanning along all the fibres. Images were acquired using both bright light and linearly polarized light and objectives of x10 and x20, leading to a maximum spatial resolution of 18 000 x 2000 pixels, with a pixel size of 328 to 656 nm. The diameters were measured at 3 to 6 spots along each fibre element by optical microscopy and the

Preprints (www.preprints.org) | NOT PEER-REVIEWED | Posted: 30 May 2023 doi:10.20944/preprints202305.2090.v1

cross-sectional area was calculated from the mean of the diameters assuming a circular cross-section. The edges of the paper frame were cut prior to the test.

2.4. Optical image processing

Optical images were processed to evaluate the density of defect within flax fibres. The process is illustrated in Figure 1. All acquired images were converted from RGB to grey level images. Image superposition is required to encapsulate the grey levels of the polarised image within the fibre element space. For such a purpose, a series of image processing operators such as threshold, fill hole, max feature isolation were used to convert the bright image into an outlined one resulting in the image of fibre boundary extraction as shown in Figure 1. Next, the retrieved boundaries from the outlined image were added and superimposed to the polarised image. The grey level distribution within the fibre delimited by the added boundaries were analysed to derive the linear density of the defects and their intensity compared to the mechanical properties.

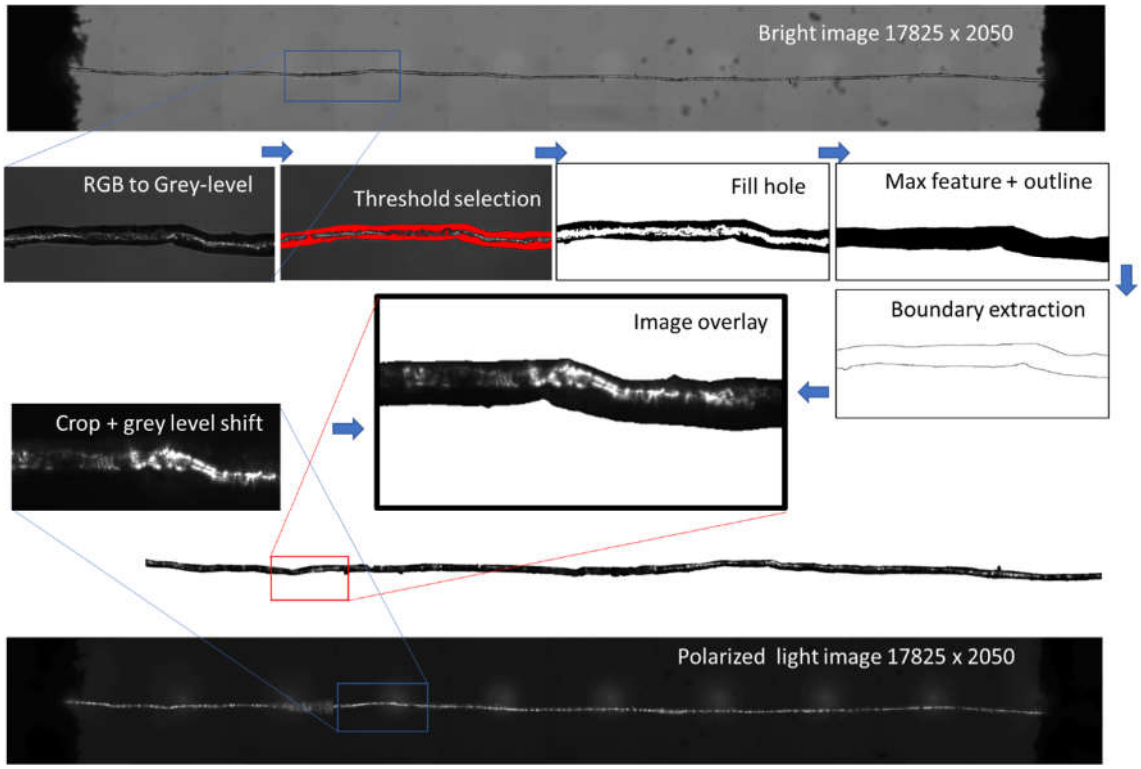

Figure 1. Image processing used to measure the density of defects from optical sources combining bright and linearly polarized lights.

2.5. Standard tensile experiments

- Unitary fibre scale:

Tensile testing experiments were carried out on unitary fibres up to the fracture point in a MTS machine (MTS System, Créteil, France) at IRDL, Lorient (France), using a 2N load cell and a strain rate of 1 mm/min, following the norm AFNOR NF T 25-501. The controlled testing environment was set to 25 ± 1°C and 48 ± 2 % of relative humidity. The fibres were extracted manually and glued on a paper frame with a gauge length of 10 mm. The edges of the paper frame were cut prior to the test. The compliance of the system was taken into account in order to compensate the influence of non-specimen extension in tensile testing leading to an under-estimation of Young's modulus and over-estimation of strain [34]. Regarding the test reliability, 45 unitary fibres were tested to ensure confidence in measured properties. The stress – strain curves are built considering the determination of the cross-sectional areas, which are based on 6 optical measurements along their length and assuming a circular approximation.

Preprints (www.preprints.org) | NOT PEER-REVIEWED | Posted: 30 May 2023 doi:10.20944/preprints202305.2090.v1

- Bundle scale:

Tensile testing experiments were carried out on 42 bundles in a MTS machine (MTS System, Créteil, France) at IRDL, Lorient (France), using a 50N load cell, an acquisition frequency of 10 Hz and a strain rate of 1 mm/min. The controlled testing environment was set to 23 ± 1°C and 43 ± 1% of relative humidity. The fibre bundles were extracted manually and glued on a paper frame with a gauge length of 75 mm. The mean diameters were determined as the mean between 6 diameter measurements along the bundles performed by optical microscopy. The edges of the paper frame were cut prior to the test.

2.6. In situ tensile experiments

Tensile testing experiments were carried out under high speed camera recording on unitary fibres using a Linkam machine TST350 (Linkam Scientific Instruments, Epsom, UK) with a 20N load cell. The tensile device was placed on a stage equipped with micrometer drives, allowing displacements with a precision in the range of the µm (Figure 2). As only the central zone was possible to image, the gauge length was adapted from 15 to 5 mm in order to capture the damage mechanisms without needing to localize the rupture. Moreover, laser markings were placed at intervals of 0.5mm on the 5 mm cardboard frame in order to recall specific locations of interest noticed during optical scanning. The testing environment was set to 24 ± 1°C and 27 ± 3 % relative humidity. Continuous tensile tests were conducted with a displacement rate of 1 mm/min according to the AFNOR standard NF T 25-501. Moreover, the displacement was applied at both jaws. At least 11 unitary fibres and 2 bundles were tested for the damage study.

High speed camera recording with speeds ranging from 100 000 to 270 000 frames per second (fps) was achieved using a Photron camera Fastcam SA1.1 type (Photron, Tokyo, Japan), equipped with a telecentric lens TC16M009 (Opto engineering, Mantova, Italy). The full frame dimensions were 1024 x 1024 pixels for frame rates up to 5400 fps. The dimensions were reduced around the fibre elements up to 1024 x 16 pixels in order to reach 270 000 fps. The pixel size is 5.1 µm with this set up. The acquisition was triggered manually as soon as the failure was observed, allowing to record the sequence before trigger. The exposure time was reduced in order to avoid blurry effects as much as possible. Additional lightening was applied to improve the image quality thanks to a LED source placed behind the tensile device (Figure 2).

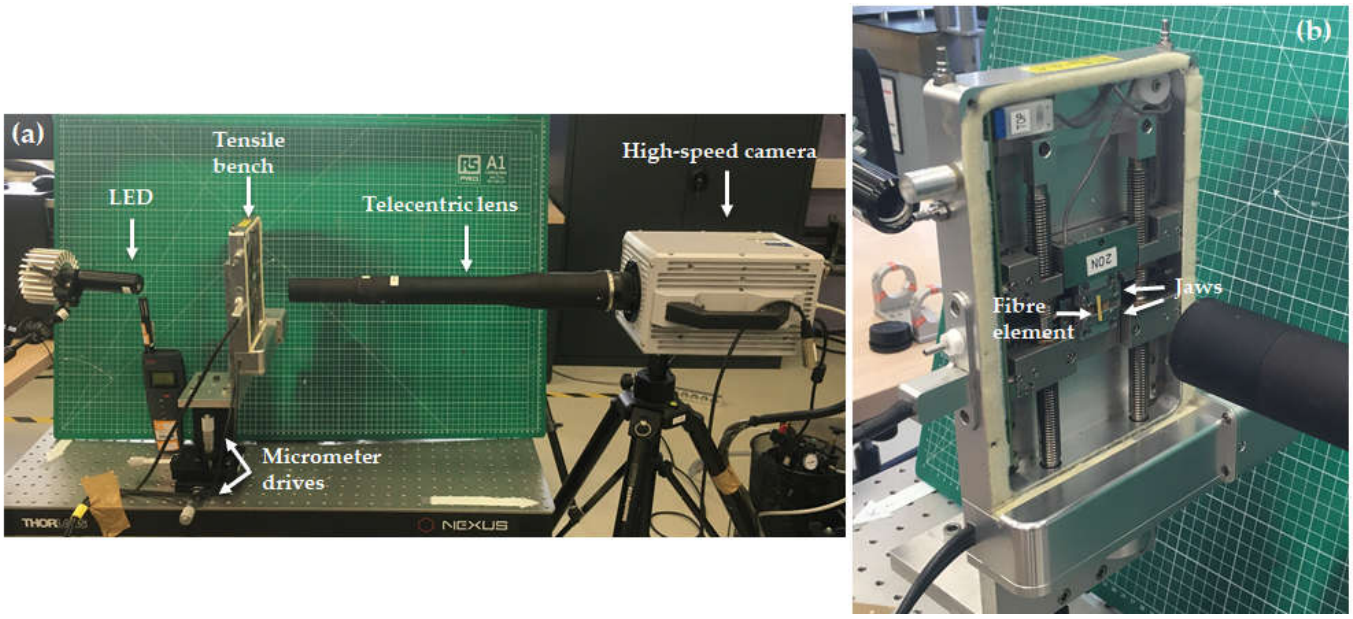

Figure 2. a) Overview of the experimental set up of high-speed imaging *in situ* tensile testing experiments. b) Magnified view of the specimen mount on the tensile machine.

 doi:10.20944/preprints202305.2090.v1

2.7. Scanning electron microscopy observations

Scanning electron microscopy (SEM) was performed on fibres elements after tensile testing close to the rupture point using a SEM Quattro S (ThermoFisher, USA). The fibre elements, still glued on the cardboard frame at their two extremities, were placed in a clamp and observations were conducted under low vacuum conditions under a pressure of 100 Pa, an acceleration voltage of 7 kV and magnification between x150 and x15 000.

3. Results and discussion

3.1. Biochemical results

The monosaccharide composition of the Bolchoï variety determined using the gas phase chromatography (GPC), and expressed as a function of dry matter shows that the main monosaccharide is glucose, which represents 78% of the dry matter. Glucose is often considered to represent the cellulose content of bast fibres, and values between 55 and 90% are reported in literature for retted textile flax [35]. Regarding the other minor in mass saccharides, the galactose content is 3.6%. Galactose is the main constituent of β(1-4)-galactan, the main encrusting component of unitary fibres, likely to be part of rhamnogalacturonan-I (RG-I) [36]. Both have been observed in the secondary cell wall at maturity. The galactose/rhamnose ratio is reported to tune the length and number of the RG-I chains, allowing to compute the cellulose microfibril packing [37]. In our study, this ratio is close to 4.8. The uronic acid content is 1.9 ± 0.1% and reflects the pectin presence of the middle lamella[38].

The lignin content is around 2.4% of the dry matter. The values are in agreement with those reported in literature, between 1 and 5% for flax [39] [3] [40]. A higher lignin rate was described by several authors [41, 42] as a possible response to an abiotic stress such as lodging, temperature or lack of water. The lignin being predominant in the middle lamella and cell junctions [43, 44], a large degree of retting and thin middle lamella might explain the relatively low lignin content in the studied flax.

The protein level was estimated from a nitrogen level assay and shows the same trend as the lignin content with a low value around 1.4%. The differences suggest that the compound middle lamella (CML), composed of the middle lamella and adjacent primary cell walls and enriched in structural proteins [45], is less important for the studied flax. However, one must take into consideration that the origin of proteins is diverse and includes both those contained in the fibres (mentioned in the CML) and those introduced by the retting step. It should be noted that a retted flax surely owes its low protein level to the fact that it underwent large enzymatic digestion, proteases being also secreted by the decomposing microorganisms. Moreover, some proteins might be involved in the plant defence mechanisms to external stresses [46].

3.2. Overall mechanical behaviour

Figure 3 shows the typical stress -strain response of the studied flax fibre at both the unitary and bundle scale. At the unitary fibre scale for which the average flax fibre diameter is 16 ± 3 µm, the average Young's modulus reflecting the compilation of 45 testing results is 40 ± 10 GPa. The observed low stiffness of the studied flax can be related to a high microfibril angle or presence of a large number of defects. The other measured properties are the elongation at break (2.04 ± 1.05 %) and the tensile strength (666 ± 232 MPa). When comparing these results with data from literature [47], the strength and stiffness are positioned in the lower range, while the elongation at break are in the middle range.

The results of tensile testing at the bundle scale show that the tensile strength is 205 ± 85 and 193 ± 92 MPa. Taking into account the mean diameter of the bundles of 114 ± 21 µm, which represents approximately 7 times the unitary fibre diameter, the large probability of critical flaws would explain a low strength value at the bundle scale according to Griffith's theory [48]. These strength scores could be attributed to a high degree of retting leading to a less cohesive middle lamella or to a more technical aspect related to the influence of the gauge length in sample testing [49]. Nevertheless, the achieved values are in agreement with the literature results for 75mm gauge length [22, 50], and the

Preprints (www.preprints.org) | NOT PEER-REVIEWED | Posted: 30 May 2023 doi:10.20944/preprints202305.2090.v1

decrease in strength as a function of the gauge length has already been studied extensively. Indeed, at gauge lengths above a threshold value of approximately 25 mm the bundles can be considered as aligned short composites driven by the weaker mechanical properties of the middle lamella. Load drops prior to the final failure were also observed as shown in Figure 3, possibly corresponding to the successive early failure of some fibres within the bundles [22-24]. The strain at break (1.24 ± 0.34 %) appears smaller than the unitary fibre scale, which supports the idea of the role of a weaker phase that drives the failure of the bundle, namely the middle lamella. Young's moduli results (19.1 ± 6.2 GPa) are obtained with a variability of about 32% (i.e., ratio between the standard deviation and the average value). This variability underlines the change in bundle diameter (18%) but also the non-linear behaviour, against which stiffness assessment is conducted in the last linear segment of the stress-strain curves prior to the load drops.

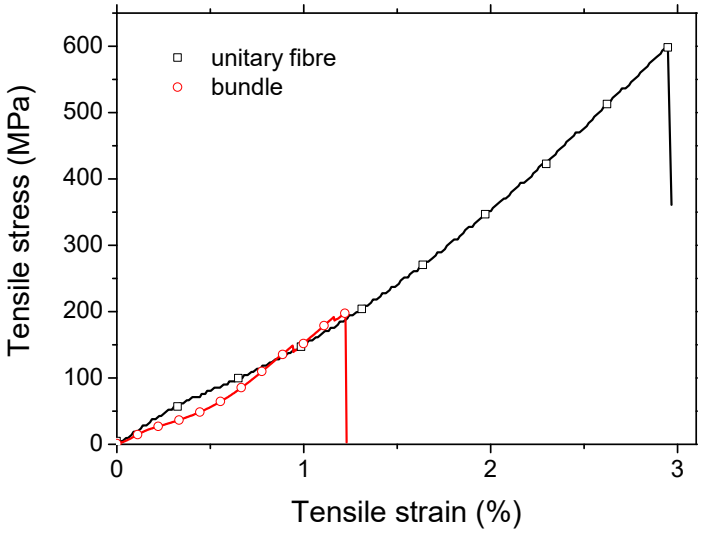

Figure 3. Typical tensile response of flax fibre elements at the unitary and bundle scale.

The relatively low score of the tensile properties at both the unitary and bundle scales can be related to the circular cross-section approximation, which can be better captured with automated laser scanning technique for instance. A correction factor similar to those determined for other types of plant fibres [51, 52] could be applied to compensate the underestimation of the fibre strength and moduli induced by the circular assumption.

3.3. Defect analysis results

Figure 4a illustrates the variation of the defect intensity along the fibre length for which the average size is 19 ± 2 μm. The defect intensity is measured here as the average grey level within the transverse direction. Within the same double Y axis plot, the variation of the fibre diameter is depicted. Large peaks reaching 32 μm indicate the presence of remains of the middle lamella. Smaller ones of about 12 μm suggest the presence of twisting which is often encountered during the sample preparation. Attempts to correlate the intensity of the defects to the diameter of the fibres seems inconclusive. Also, it seems that the average defect intensity within the entire fibre does not fit the mechanical data as for instance a large scatter is observed with the tensile strength. However, the measured scatter which represents the standard deviation of the defect density divided by the average defect intensity shows a trend with respect to the ultimate properties. The highest scatter seems to be associated with lower tensile stress values.

Preprints (www.preprints.org) | NOT PEER-REVIEWED | Posted: 30 May 2023 doi:10.20944/preprints202305.2090.v1

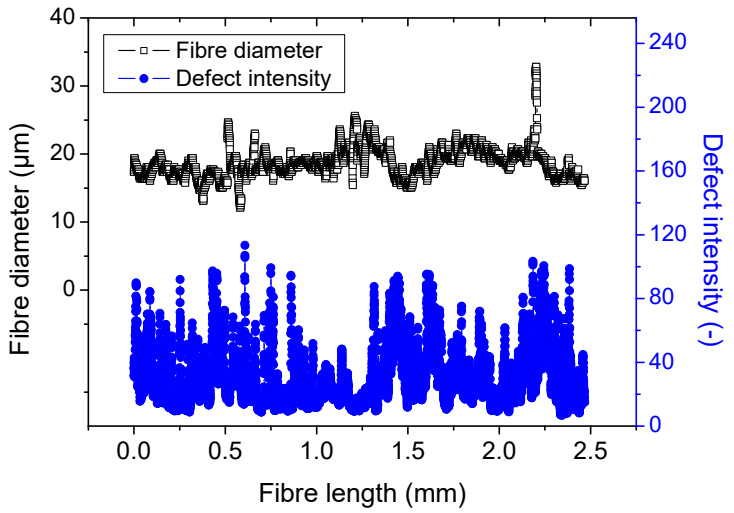

(a)

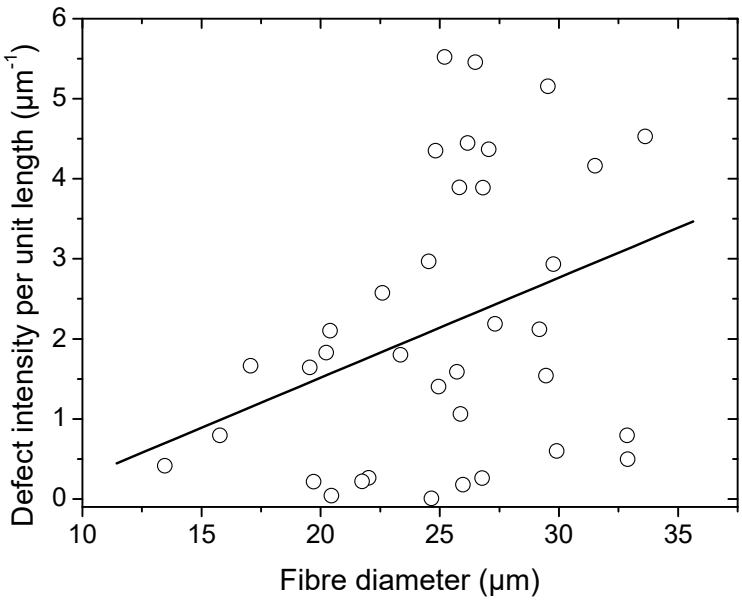

(b)

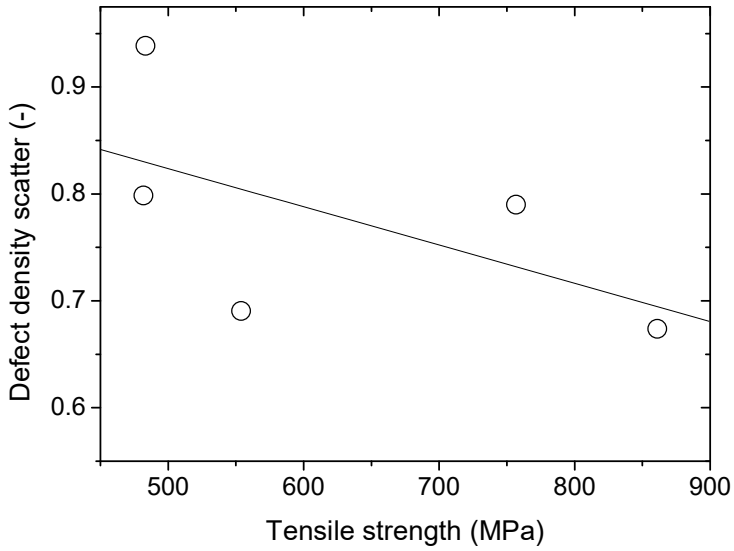

(c)

Preprints (www.preprints.org) | NOT PEER-REVIEWED | Posted: 30 May 2023 doi:10.20944/preprints202305.2090.v1

Figure 4. Defect analysis from optical imaging: (a) linear density of the defects measured according to the average grey level divided by the diameter, (b) correlation between the defect density and the fibre diameter, (c) relationship between tensile strength and defect density. .

Figure 4b shows the compiled defect density results for 45 unitary fibres as a function of the average diameter. The diameter is measured along the entire length as shown in Figure 1 by processing outline images from the bright optical micrographs. The defect density is depicted as the average grey level intensity from optical images acquired under linearly polarized light. Figure 4b shows that there is a large scatter in the results but a global trend supporting the idea of an increased defect density with an increasing fibre diameter still can be read. The scatter also increases with the increase of the diameter, which can be also related to the difficulty to capture the defect within the fibre cross-section if this one is not rotated during the acquisition.

When relating these data to the tensile behaviour, there is unfortunately no general trend between the defect density and the tensile response. Figure 4c shows, however, a negative correlation between the tensile strength and the scatter in defect density. This scatter is measured as the ratio between the standard deviation and the average defect density along the length of unitary fibres.

3.4. In-situ mechanical behaviour at unitary fibre scale

Detailed characteristics and mechanical properties resulting from *in situ* tensile testing of flax unitary fibres and bundles with high speed camera recording are presented in Table 1. The failure sequences were reported thanks to a high-speed camera, with recording speed ranging from 108 000 to 270 000 frames per second (fps). Images at the initial stage, prior and after failure were compared to the initial image obtained under bright and polarized light microscopy prior to testing. SEM images of the fracture surfaces after tensile testing are also presented.

Table 1. Characteristics and mechanical properties of unitary fibres (a) and bundles (b) after high speed camera *in situ* tensile testing. ROI: Region Of Interest.

Sample	Recording speed (fps)	ROI size (pix.)	Strength (MPa)	Elongation at break (%)
b-1-41	100 000	704 x 48	403	1.80
a-1-10	108 000	1024 x 48	757	3.19
a-1-11			557	3.76
b-1-37			794	3.45
a-1-12	150 000	1024 x 32	482	3.60
a-1-13			875	1.79
a-1-14			554	2.78
a-1-22			483	3.97
a-1-16			852	1.59
a-1-18			861	3.57
a-1-20	270 000	1024 x 16	462	0.80
a-1-24			595	1.39
a-1-26			741.3	4.17
Mean values for unitary fibres	-	-	656 ± 164	2.78 ± 1.18

The tensile strengths and elongation at break of unitary fibres are close to the values obtained for regular tensile experiments for a gauge length of 10mm, with a mean strength of 656 ± 164 MPa and a mean strain at break of 2.78 ± 1.18 % even if only 11 fibres were tested here.

The complementary observations lead to different failure scenarios depending on the fibre, displayed in Figures 5 to 9. In particular, fracture fibre ends underline a fully transverse failure propagation in Figure 6 or a combination of transverse and longitudinal propagations at different degrees in other cases (Figures 5, 7-8, and 9). Moreover, the small recording periods down to 3.7 µs did not allow to get consecutive images of the failure mechanisms in the case of almost fully

Preprints (www.preprints.org) | NOT PEER-REVIEWED | Posted: 30 May 2023 doi:10.20944/preprints202305.2090.v1

transverse failure (Figures 5 and 6), suggesting a very unstable system and transverse crack propagation speeds higher than 1.5 and 4 m/s respectively. The longitudinal deviation might thus lead to a slower overall failure, acting as an energy dissipating mechanism as hypothesized by Beaugrand et al. [53]. However, the observations at the surface only prevent to capture the crack propagation occurring in the bulk. Moreover, one has to recall that only 5 fibres were fully described here.

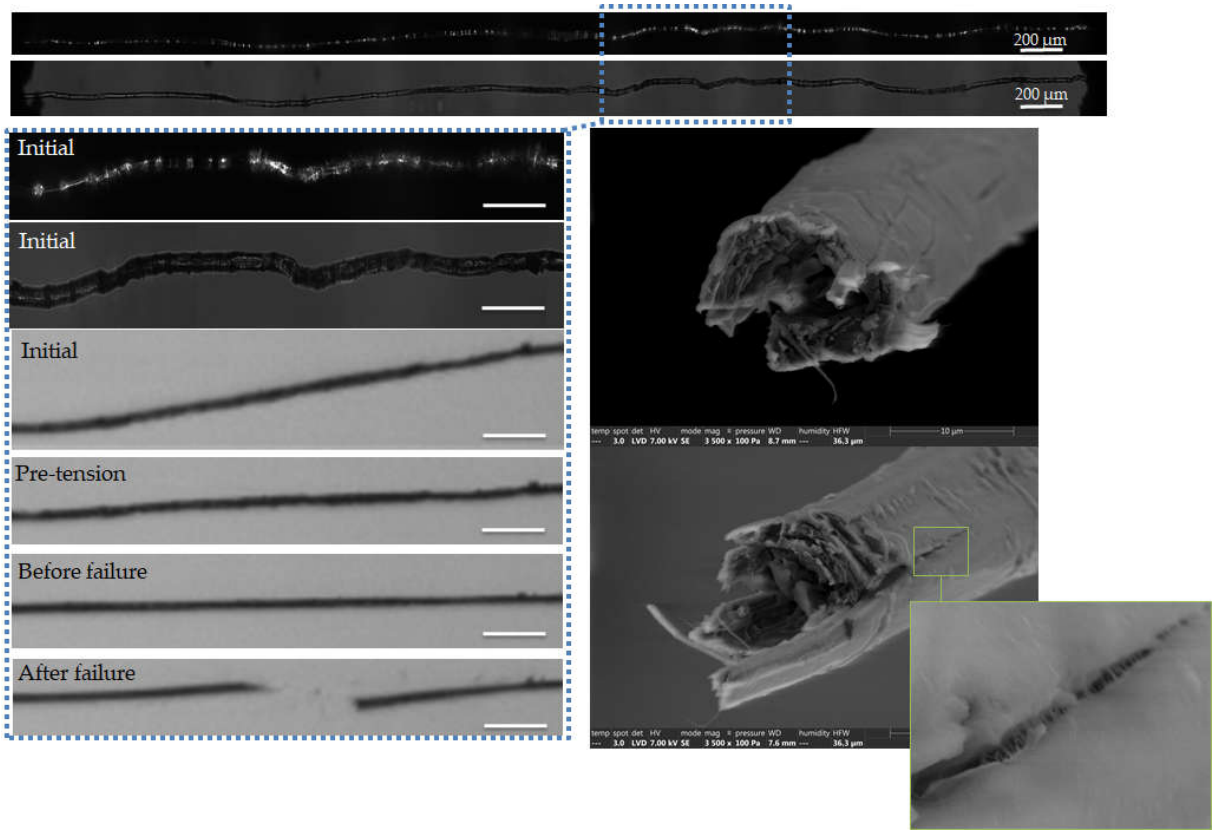

Figure 5. Images of the initial stage observed by optical microscopy under both bright and polarized light, and zoom on the steps of failure of a flax unitary fibre **a-1-11,** observed during *in situ* tensile testing thanks to a high-speed camera. SEM images of the two fracture surfaces after complete failure. The scalebars indicate 100 µm unless specified.

Preprints (www.preprints.org) | NOT PEER-REVIEWED | Posted: 30 May 2023 doi:10.20944/preprints202305.2090.v1

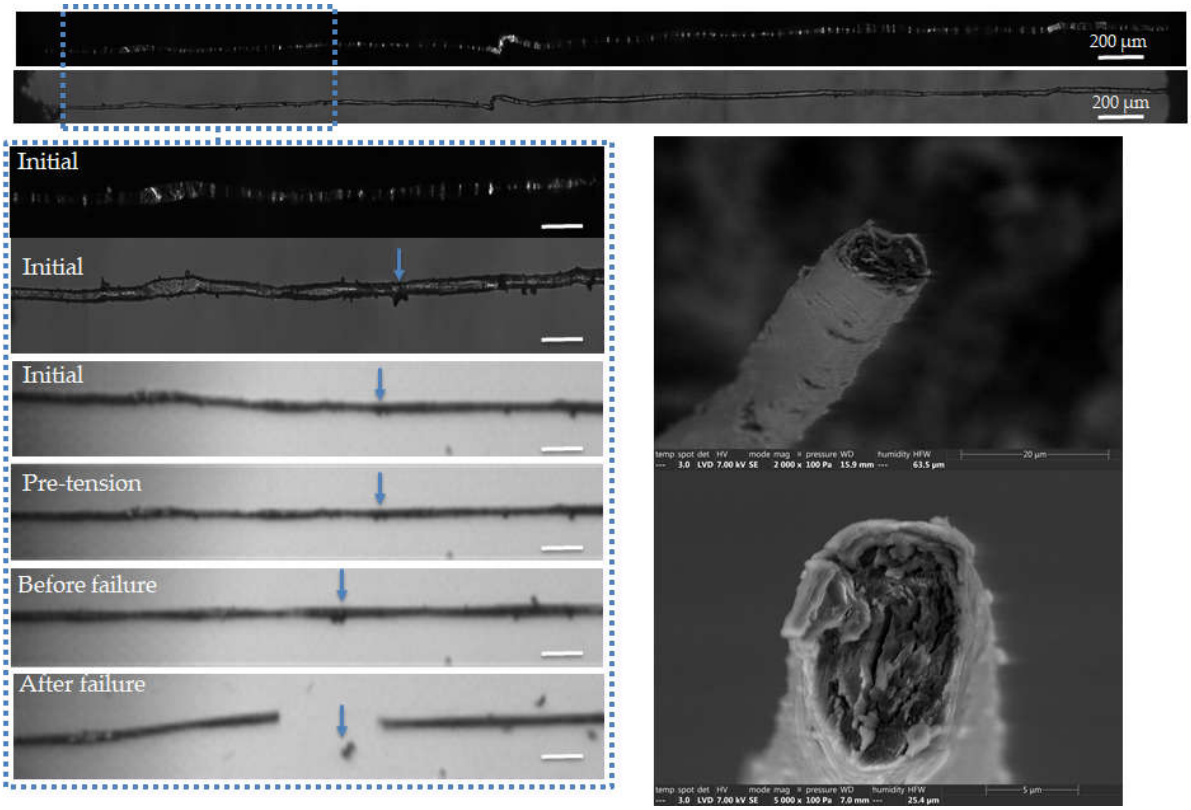

Figure 6. Images of the initial stage observed by optical microscopy under both bright and polarized light, and zoom on the steps of failure of a flax unitary fibre **a-1-22**, observed during *in situ* tensile testing thanks to a high-speed camera. SEM images of the two fracture surfaces after complete failure. The scalebars represent 100 µm unless specified and the separation of a surface impurity is indicated by blue arrows.

Preprints (www.preprints.org) | NOT PEER-REVIEWED | Posted: 30 May 2023 doi:10.20944/preprints202305.2090.v1

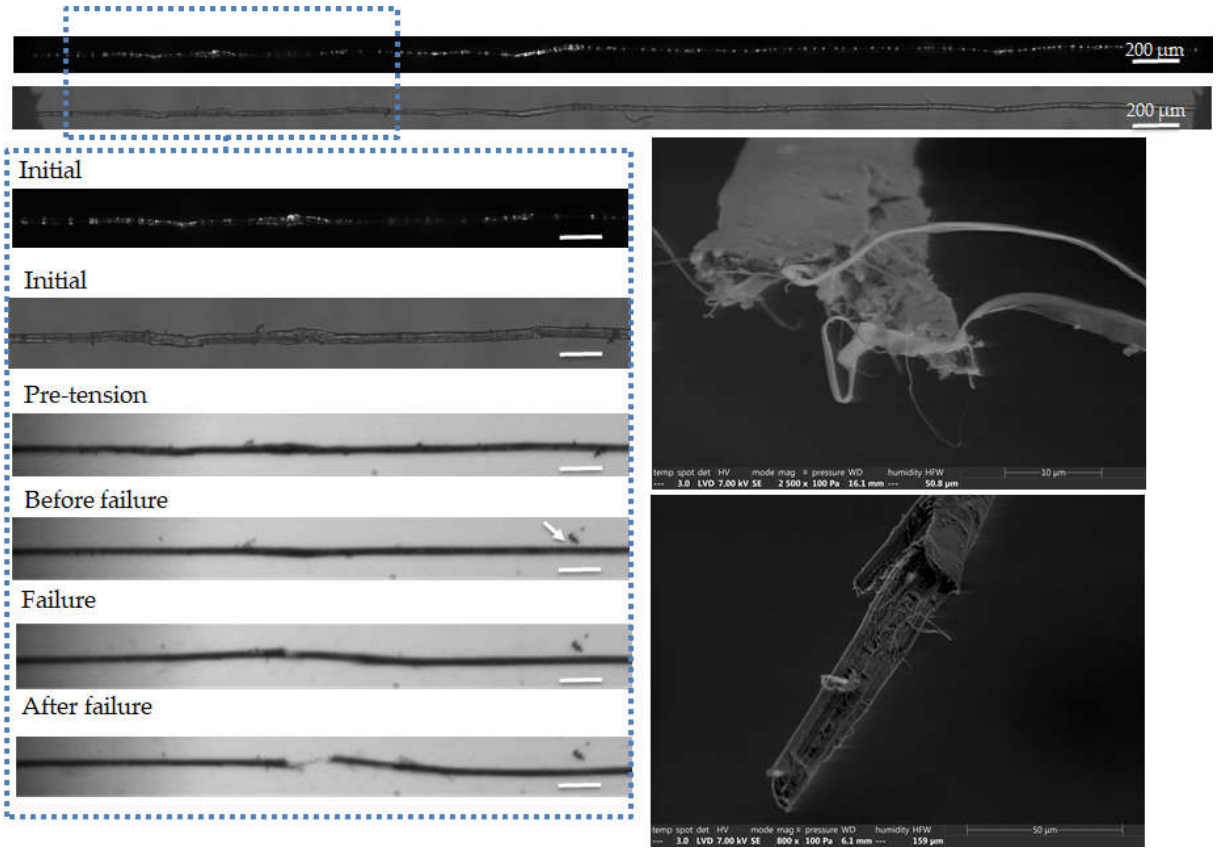

Figure 7. Images of the initial stage observed by optical microscopy under both bright and polarized light, and zoom on the steps of failure of a flax unitary fibre **a-1-14**, observed during in situ tensile testing thanks to a high-speed camera. SEM images of the two fracture surfaces after complete failure. The scale bars represent 100 µm and the separation of a surface impurity is indicated by a white arrow.

Preprints (www.preprints.org) | NOT PEER-REVIEWED | Posted: 30 May 2023 doi:10.20944/preprints202305.2090.v1

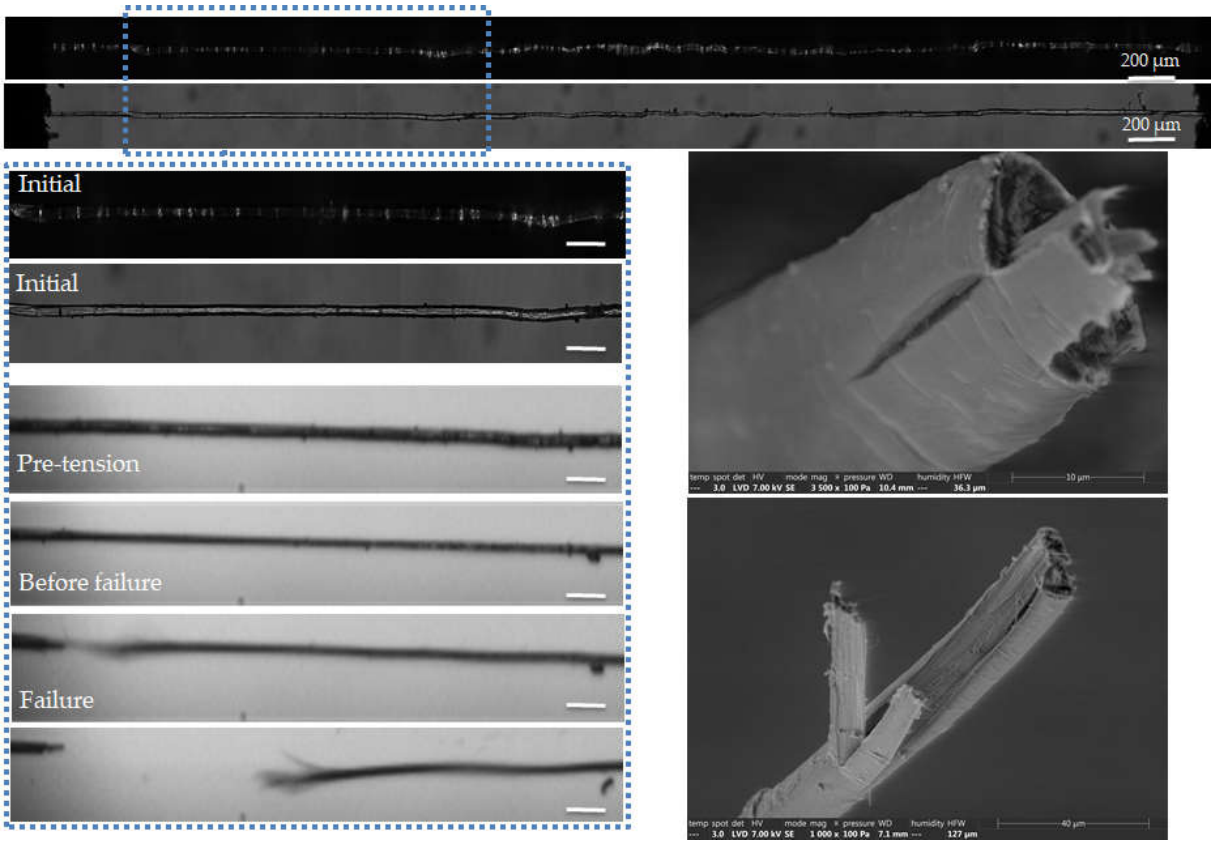

Figure 8. Images of the initial stage observed by optical microscopy under both bright and polarized light, and zoom on the steps of failure of a flax unitary fibre **a-1-18**, observed during *in situ* tensile testing thanks to a high-speed camera. SEM images of the two fracture surfaces after complete failure. The scalebars represent 100 µm.

Preprints (www.preprints.org) | NOT PEER-REVIEWED | Posted: 30 May 2023 doi:10.20944/preprints202305.2090.v1

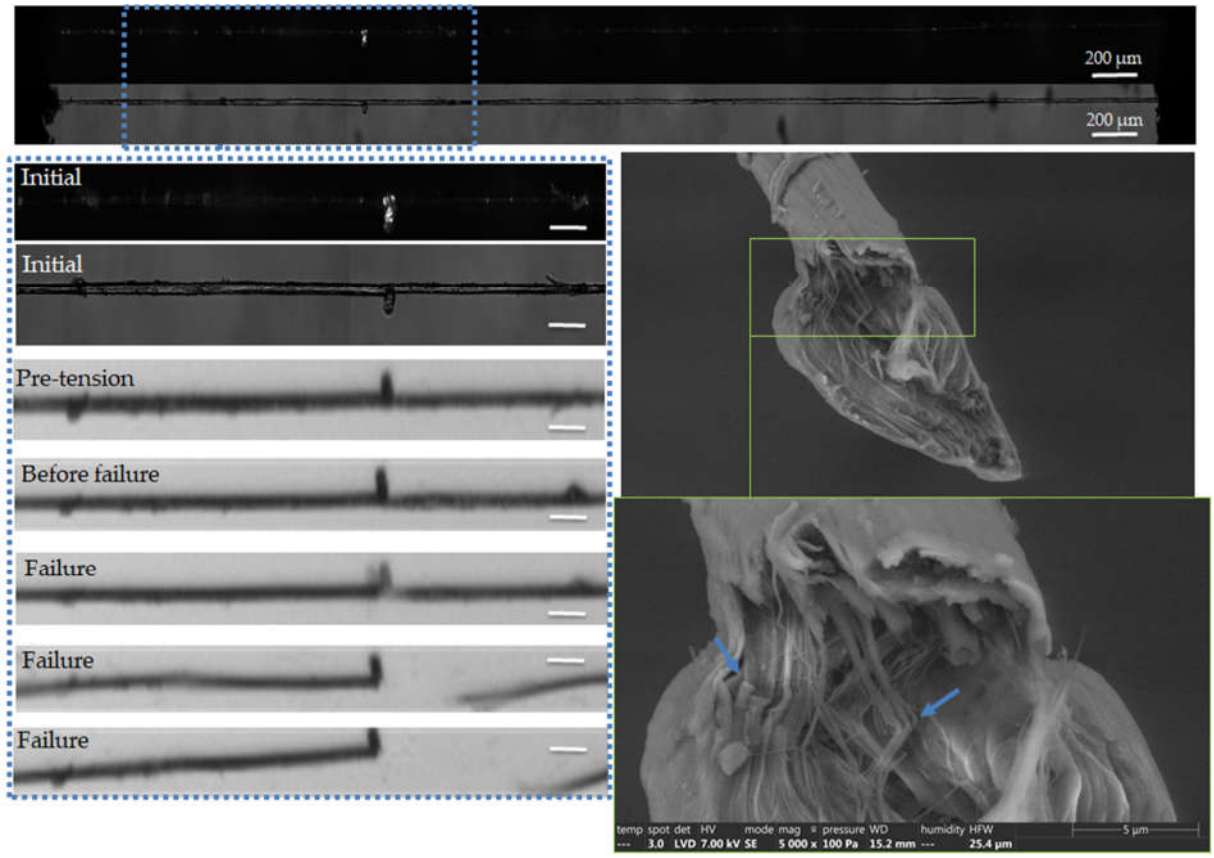

Figure 9. Images of the initial stage observed by optical microscopy under both bright and polarized light, and zoom on the steps of failure of a flax unitary fibre **a-1-20**, observed during *in situ* tensile testing thanks to a high-speed camera. SEM images of the fracture surface of the left part of the fibre after complete failure. The scalebars represent 100 µm and mesofibrils misorientations highlighting a defected area are indicated by blue arrows.

In Figure 5, we notice a rupture occurring in a defected part of the fibre, which appears as a bright and curved area under polarized light prior to loading. However, the precise location of failure initiation is difficult to evaluate and we can therefore only assess the failure initiation in a globally defected area. The fracture surfaces reveal a major transverse failure with a minor longitudinal deviation which could be attributed to a sublayer delamination or the presence of a central lumen [54]. Finally, longitudinal cracks close to the fracture surface can be underlined, with a zoom on a crack bridging phenomenon.

The fracture surfaces of Figure 6 also show a predominant transverse failure, revealing a central dark area which could correspond to the lumen. Moreover, the possible implication of surface mechanisms is evidenced on the high-speed camera images, with a failure occurring close to a surface impurity evidenced by blue arrows. The latter could be remainings from residual middle lamella or cortical tissues. Interestingly, the failure did not occur on the curved area observed initially, which is progressively deployed upon tensile testing.

A transverse cracking followed by a major longitudinal crack propagation is highlighted on the SEM images of Figure 7. Moreover, we notice the failure occurring in a zone of higher fibre diameter appearing as a bright area under polarized light. It could be the result of processing damage prior to the test due to the compression of the cell walls between rollers [55]. Moreover, we can observe the removal of a surface impurity evidenced by a white arrow on the right part of the fibre. Regarding the fracture surfaces, a major longitudinal crack is evidenced on the upper image, as well as disorganized cellulose macrofibrils.

The combination of transverse and longitudinal mechanisms is highlighted on the SEM images of Figure 8. The failure does not occur in the brightest area, and therefore zone of higher defect

 doi:10.20944/preprints202305.2090.v1

density along the fibre. The fracture surfaces reveal an important crack at the surface of the fibre upper part, and a cell wall split longitudinally in three parts on the lower part of the fibre.

Finally, the fibre displayed in Figure 9 shows a failure close to a protrusion present at the surface. It could be attributed at first sight to a remaining part of adhering tissue, arguably from the middle lamella or cortical tissues. However, the fracture surface depicts the presence of cellulose macro and microfibrils close to this protrusion, with misalignment characteristic of a defect which could have driven the failure [56]. Unfortunately, the observation of the other part of the fibre was not possible to strengthen the hypothesis. Moreover, the very low defect content and straight fibres observed at the initial stage prior to loading could be the result of a pre-tension applied during the sample preparation, explaining the low strain at break value of 0.8%.

In conclusion, the careful observation of failure sequences in 5 different unitary fibres reveals different mechanisms involving pure transverse and therefore more brittle failure or a combination of transverse failure and longitudinal splitting, in agreement with previously results reported in literature [27, 28, 57]. Fracturographic analysis reveals rough surfaces typically encountered after tensile solicitation [24], and the presence of cracks close to the fracture surface. Moreover, some fibres have been witnessed to fail in a zone of high defect density evidenced under polarized light microscopy, but the scenario cannot be generalized to all samples. In agreement with the explanation put forward by Madsen et al. [57], the failure mechanisms might be dependent on microstructural parameters such as the severity and distance between defects as well as the lumen size. Therefore, the differences between the fibres and correlation to their mechanical properties are difficult to explain based only on the surface information provided in this study. The use of X-ray tomography will be of interest to access bulk information and especially defect severity and porosity-related mechanisms in the second part of the study. Finally, the possible implication of surface contaminants to the failure initiation is underlined in two cases. As evidenced in Figure 9, the surface flaws might coincide with zones of cellulose microfibril misalignment too. As a prospect, bulk information will help to confirm and understand the underlying mechanisms.

3.5. In-situ mechanical behaviour at bundle scale

The investigation is further conducted at the bundle scale to better understand the contribution of the middle lamella to the failure mechanisms. Two bundles reflecting contrasted behaviour are displayed in Figure 10 and Figure 11. The first bundle presents a hierarchical failure sequence characterized by delamination between the fibres followed by the transverse failure of some unitary fibres (Figure 10). It agrees with the observations of several authors [22-24] referencing splitting of the fibres before complete failure. Details of the rough interface are observed on the SEM images, with residual compound middle lamella and fibrillar structure which might correspond to cellulose macrofibrils of the outer layers. In contrast, a predominant transverse failure of the unitary fibres without delamination is observed in Figure 11. It occurred in a thicker zone which might correspond to a defected area. However, polarized light microscopy did not permit the observation of defects in thick bundles, and volume information will help decipher the role of porosity and initial delamination in the difference of behaviours. Indeed, the second scenario lead to an early failure characterized by a lower strength and strain at break (around 400 MPa and 1.8% compared to 794 MPa and 3.5% reported for the first bundle). The value of 800 MPa for the strength agrees with values reported for such low gauge length by Bos et al. [58]. As hypothesized by Fuentes et al. [14], the biochemical composition of the middle lamella might also explain differences between the failure scenarios. However, one has to recall that the gauge length is inferior to most fibre lengths. Therefore, the behaviours observed here might not reflect the solicitation of the middle lamella as for important gauge length, but rather resemble the behaviour of the unitary fibre scale.

Preprints (www.preprints.org) | NOT PEER-REVIEWED | Posted: 30 May 2023 doi:10.20944/preprints202305.2090.v1

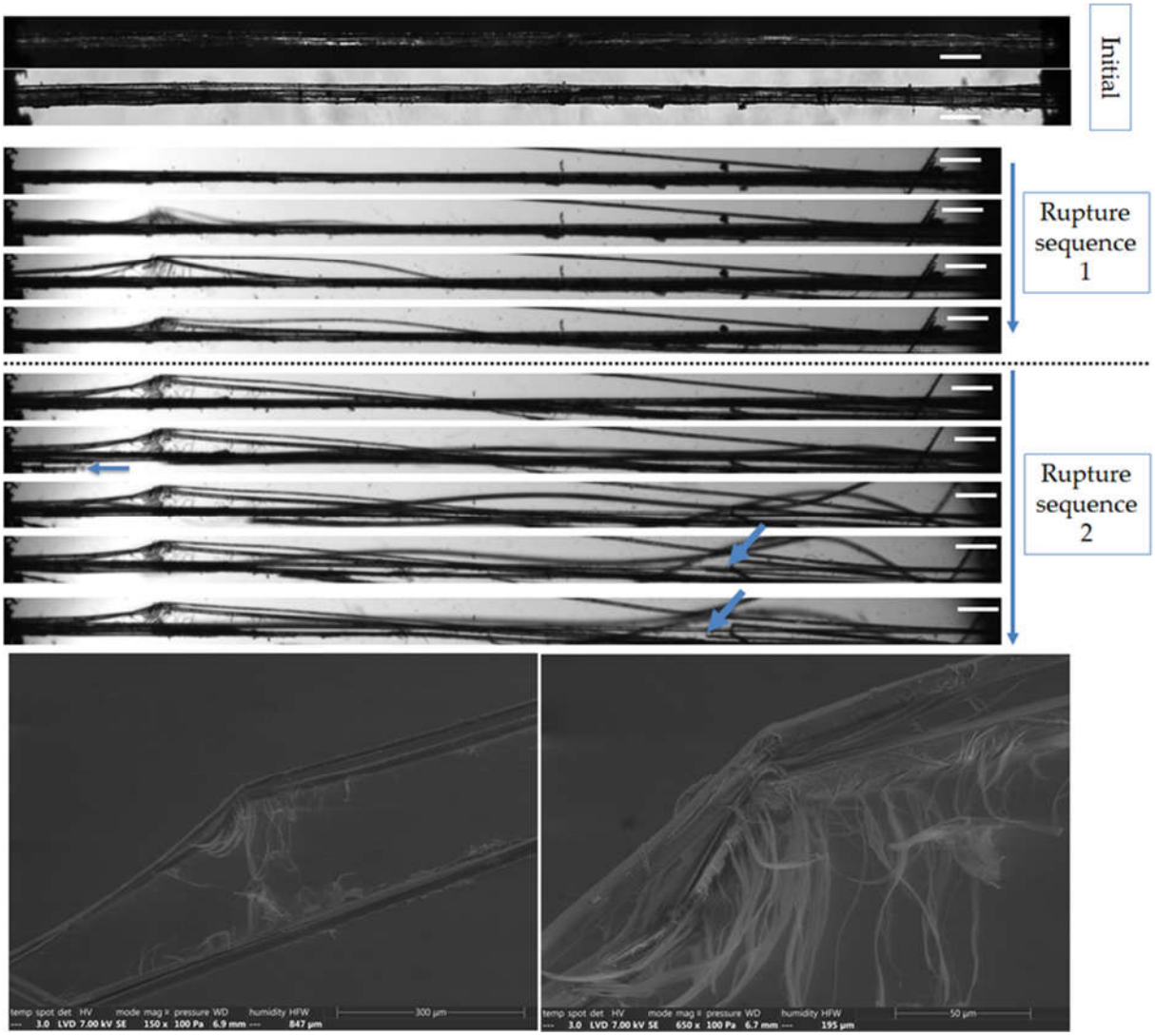

Figure 10. Top: Images of the initial stage observed by optical microscopy under both bright and polarized light, and zoom on the two consecutive failure sequence of a flax bundle **b-1-37**, observed during *in situ* tensile testing thanks to a high-speed camera. Bottom: SEM images taken along the bundle after complete failure. The scale bars represent 200 µm unless specified and the blue arrows indicates transverse failure of unitary fibres.

Preprints (www.preprints.org) | NOT PEER-REVIEWED | Posted: 30 May 2023 doi:10.20944/preprints202305.2090.v1

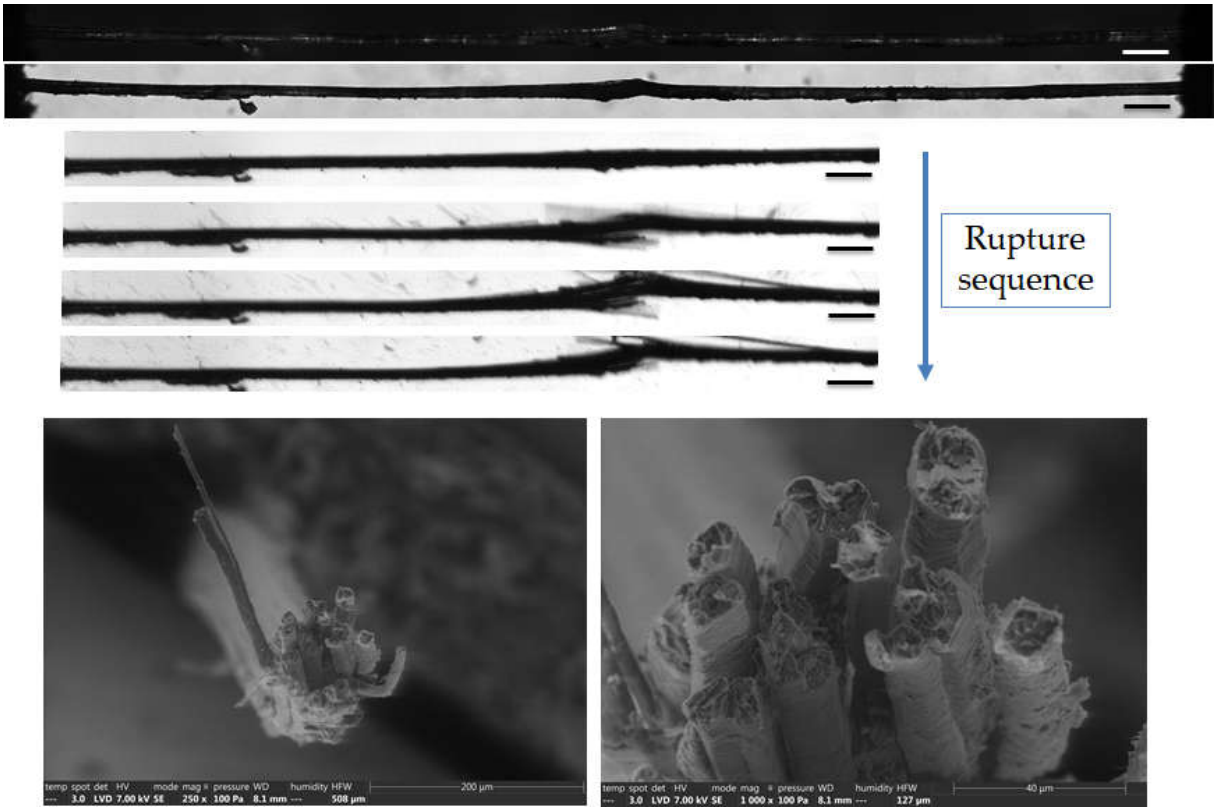

Figure 11. Top: Images of the initial stage observed by optical microscopy under both bright and polarized light, and zoom on the failure sequence of a flax bundle b-1-41, observed during *in situ* tensile testing thanks to a high-speed camera. Bottom: SEM fracture surface of one extremity after complete failure. The scalebars represent 200 µm unless specified.

4. Conclusions

High-speed camera observations upon tensile testing highlighted the fastest purely transverse failure of some unitary fibres and a combination of transverse and longitudinal propagation for others, resulting in a delayed failure. The polarized light microscopy revealed a possible implication of defects, and bright light observations shed the light on the possible role of surface effects. However, the underlying mechanisms might be linked to porosity and need further investigation that can be performed using more adequate tools such as X-ray tomography. Indeed, surface observation can hardly reveal the extent of the lumen role in driving or contributing to the failure at the unitary fibre scale, where predominant transverse failure.

Contrasted behaviours are witnessed at the bundle scale, linked to the additional complexity induced by the presence of numerous fibres linked by a middle lamella. Indeed, high speed camera showed a hierarchical failure by delamination between the fibres followed by transverse failure of the unitary fibres in one case, and purely transverse rupture of fibres close to a defected area in another case. The bulk effects can be again further explained by X-ray tomography experiments, which will be the subject of a future work. The idea is to provide realistic scenarios of the transverse rupture for both compact and airy bundles considering the role of the middle lamella.

Acknowledgments: The authors would like to express their gratitude to Antoine Kervoelen from Université Bretagne Sud, Lorient, France for his technical assistance in preparing mechanical testing of fibre samples. The authors extend their gratitude to Depestele company, France for providing fibre samples. The authors also thank the INTERREG VA FCE Program, FLOWER project, Grant Number 23, for the funding of this work.

References

[1] Rahman MZ. Mechanical and damping performances of flax fibre composites – A review. Composites Part C: Open Access. 2021;4.

[2] Baley C, Bourmaud A, Davies P. Eighty years of composites reinforced by flax fibres: A historical review. Composites Part A: Applied Science and Manufacturing. 2021;144.

[3] Bourmaud A, Beaugrand J, Shah DU, Placet V, Baley C. Towards the design of high-performance plant fibre composites. Progress in Materials Science. 2018;97:347-408.

[4] Thomason JL, Carruthers J, Kelly J, Johnson G. Fibre cross-section determination and variability in sisal and flax and its effects on fibre performance characterisation. Composites Science and Technology. 2011;71(7):1008-15.

[5] Melelli A, Durand S, Alvarado C, Kervoëlen A, Foucat L, Grégoire M, et al. Anticipating global warming effects: A comprehensive study of drought impact of both flax plants and fibres. Industrial Crops and Products. 2022;184.

[6] Melelli A, Durand S, Arnould O, Richely E, Guessasma S, Jamme F, et al. Extensive investigation of the ultrastructure of kink-bands in flax fibres. Industrial Crops and Products. 2021;164.

[7] Hernandez-Estrada A, Reza M, Hughes M. The Structure of Dislocations in Hemp (Cannabis sativa L.) Fibres and Implications for Mechanical Behaviour. BioResources. 2020;15:2579-95.

[8] Zhang H, Sui T, Thygesen LG, O'brien P, Korsunsky A. Multi-modal Microscopy Characterisation of Nodal Markings in Flax Fibre. World Congress on Engineering London2015.

[9] Bourmaud A, Pinsard L, Guillou E, De Luycker E, Fazzini M, Perrin J, et al. Elucidating the formation of structural defects in flax fibres through synchrotron X-ray phase-contrast microtomography. Industrial Crops and Products. 2022;184.

[10] Quereilhac D, Pinsard L, Guillou E, Fazzini M, De Luycker E, Bourmaud A, et al. Exploiting synchrotron X-ray tomography for a novel insight into flax-fibre defects ultrastructure. Industrial Crops and Products. 2023;198.

[11] Thygesen LG, Gierlinger N. The molecular structure within dislocations in Cannabis sativa fibres studied by polarised Raman microspectroscopy. Journal of Structural Biology. 2013;182(3):219-25.

[12] Richely E, Nuez L, Pérez J, Rivard C, Baley C, Bourmaud A, et al. Influence of defects on the tensile behaviour of flax fibres: Cellulose microfibrils evolution by synchrotron X-ray diffraction and finite element modelling. Composites Part C: Open Access. 2022;9.

[13] Nilsson T, Gustafsson PJ. Influence of dislocations and plasticity on the tensile behaviour of flax and hemp fibres. Composites Part A: Applied Science and Manufacturing. 2007;38(7):1722-8.

[14] Fuentes CA, Willekens P, Petit J, Thouminot C, Müssig J, Trindade LM, et al. Effect of the middle lamella biochemical composition on the non-linear behaviour of technical fibres of hemp under tensile loading using strain mapping. Composites Part A: Applied Science and Manufacturing. 2017;101:529-42.

[15] Téraube O, Gratier L, Agopian J-C, Pucci MF, Liotier P-J, Hajjar-Garreau S, et al. Elaboration of hydrophobic flax fibers through fluorine plasma treatment. Applied Surface Science. 2023;611.

[16] Rask M, Madsen B, Sørensen BF, Fife JL, Martyniuk K, Lauridsen EM. In situ observations of microscale damage evolution in unidirectional natural fibre composites. Composites Part A: Applied Science and Manufacturing. 2012;43(10):1639-49.

[17] Baley C, Perrot Y, Busnel F, Guezenoc H, Davies P. Transverse tensile behaviour of unidirectional plies reinforced with flax fibres. Materials Letters. 2006;60(24):2984-7.

[18] Van de Weyenberg I, Ivens J, De Coster A, Kino B, Baetens E, Verpoest I. Influence of processing and chemical treatment of flax fibres on their composites. Composites Science and Technology. 2003;63(9):1241-6.

[19] Le Duigou A, Kervoelen A, Le Grand A, Nardin M, Baley C. Interfacial properties of flax fibre–epoxy resin systems: Existence of a complex interphase. Composites Science and Technology. 2014;100:152-7.

[20] Charlet K, Beakou A. Interfaces within flax fibre bundle: Experimental characterization and numerical modelling. Journal of Composite Materials. 2013;48(26):3263-9.

[21] Charlet K, Béakou A. Mechanical properties of interfaces within a flax bundle – Part I: Experimental analysis. International Journal of Adhesion and Adhesives. 2011;31(8):875-81.

[22] Romhany G, Karger-Kocsis J, Czigany T. Tensile Fracture and Failure Behavior of Technical Flax Fibers. Journal of Applied Polymer Science. 2003;90:3638 - 45.

[23] Barbulée A, Jernot J-P, Bréard J, Gomina M. Damage to flax fibre slivers under monotonic uniaxial tensile loading. Composites Part A: Applied Science and Manufacturing. 2014;64:107-14.

[24] Ahmed S, Ulven C. Dynamic In-Situ Observation on the Failure Mechanism of Flax Fiber through Scanning Electron Microscopy. Fibers. 2018;6(1).

[25] Mott L, Shaler SM, Groom L, Liang B. The tensile testing of individual wood fibers using environmental scanning electron microscopy and video image analysis. Tappi Journal. 1995;78:143-8.

[26] Baley C. Influence of kink bands on the tensile strength of flax fibers. Journal of Materials Science. 2004;39:331 - 4.

[27] Aslan M, Chinga-Carrasco G, Sørensen BF, Madsen B. Strength variability of single flax fibres. Journal of Materials Science. 2011;46(19):6344-54.
[28] Beaugrand J, Guessasma S. Scenarios of crack propagation in bast fibers: Combining experimental and finite element approaches. Composite Structures. 2015;133:667-78.
[29] Silva FdA, Zhu D, Mobasher B, Soranakom C, Toledo Filho RD. High speed tensile behavior of sisal fiber cement composites. Materials Science and Engineering: A. 2010;527(3):544-52.
[30] Blakeney AB, Harris PJ, Henry RJ, Stone BA. A simple and rapid preparation of alditol acetates for monosaccharide analysis. Carbohydrate Research. 1983;113:291-9.
[31] Thibault JF. Automatisation du dosage des substances pectiques par la methode au meta-hydroxydiphenyl. Lebensmittel - Wissenschaft + Technologie Food science + technology. 1979;12:247-51.
[32] Hatfield R, Fukushima RS. Can Lignin Be Accurately Measured? Crop Science. 2005;45(3):832-9.
[33] Mariotti F, Tomé D, Mirand P. Converting Nitrogen into Protein – Beyond 6.25 and Jones' Factors. Critical Reviews in Food Science and Nutrition. 2008;48:177-84.
[34] Turek DE. On the tensile testing of high modulus polymers and the compliance correction. Polymer Engineering And Science. 1993;33(6):328-33.
[35] Richely E, Bourmaud A, Placet V, Guessasma S, Beaugrand J. A critical review of the ultrastructure, mechanics and modelling of flax fibres and their defects. Progress in Materials Science. 2021.
[36] Morvan C, Andème-Onzighi C, Girault R, Himmelsbach DS, Driouich A, Akin DE. Building flax fibres: more than one brick in the walls. Plant Physiology and Biochemistry 2003;41:935-44.
[37] Chemikosova SB, Pavlencheva NV, Gur'yanov OP, Gorshkova TA. The effect of soil drought on the phloem fiber development in long-fiber flax. Russian Journal of Plant Physiology. 2006;53(5):656-62.
[38] Gautreau M, Durand S, Paturel A, Le Gall S, Foucat L, Falourd X, et al. Impact of cell wall non-cellulosic and cellulosic polymers on the mechanical properties of flax fibre bundles. Carbohydrate Polymers. 2022;291.
[39] Faruk O, Bledzki AK, Fink H-P, Sain M. Biocomposites reinforced with natural fibers: 2000–2010. Progress in Polymer Science. 2012;37(11):1552-96.
[40] Thygesen A, Madsen B, Bjerre AB, Lilholt H. Cellulosic Fibers: Effect of Processing on Fiber Bundle Strength. Journal of Natural Fibers. 2011;8(3):161-75.
[41] Frei M. Lignin: characterization of a multifaceted crop component. ScientificWorldJournal. 2013;2013:436517.
[42] Cabane M, Afif D, Hawkins S. Lignins and Abiotic Stresses. Lignins - Biosynthesis, Biodegradation and Bioengineering2012. p. 219-62.
[43] Akin DE, Gamble GR, Morrison WH, Rigsby L. Chemical and Structural Analysis of Fibre and Core Tissues from Flax. Journal for the Science of Food and Agriculture. 1996;72:155-65.
[44] Gorshkova T. Composition and Distribution of Cell Wall Phenolic Compounds in Flax (Linum usitatissimum L.) Stem Tissues. Annals of Botany. 2000;85(4):477-86.
[45] Djemiel C, Goulas E, Badalato N, Chabbert B, Hawkins S, Grec S. Targeted Metagenomics of Retting in Flax: The Beginning of the Quest to Harness the Secret Powers of the Microbiota. Front Genet. 2020;11:581664.
[46] Corbin C, Drouet S, Markulin L, Auguin D, Laine E, Davin LB, et al. A genome-wide analysis of the flax (Linum usitatissimum L.) dirigent protein family: from gene identification and evolution to differential regulation. Plant Mol Biol. 2018;97(1-2):73-101.
[47] Baley C, Bourmaud A. Average tensile properties of French elementary flax fibers. Materials Letters. 2014;122:159-61.
[48] Griffith AA. The phenomena of rupture and flow in solids Philosophical Transactions od the Royal Society of London Series A, Containing Papers of a Mathematical of Physical Character. 1921;221:163-98.
[49] Bourmaud A, Nuez L, Goudenhooft C, Baley C. Multi-scale mechanical characterization of flax fibres for the reinforcement of composite materials. Handbook of Natural Fibres2020. p. 205-26.
[50] Alix S, Lebrun L, Marais S, Philippe E, Bourmaud A, Baley C, et al. Pectinase treatments on technical fibres of flax: Effects on water sorption and mechanical properties. Carbohydrate Polymers. 2012;87(1):177-85.
[51] Garat W, Corn S, Le Moigne N, Beaugrand J, Bergeret A. Analysis of the morphometric variations in natural fibres by automated laser scanning: Towards an efficient and reliable assessment of the cross-sectional area. Composites Part A: Applied Science and Manufacturing. 2018;108:114-23.
[52] Summerscales J, Virk AS, Hall W. Fibre area correction factors (FACF) for the extended rules-of-mixtures for natural fibre reinforced composites. Materials Today: Proceedings. 2020;31.
[53] Beaugrand J, Guessasma S, Maigret JE. Damage mechanisms in defected natural fibers. Scientific Reports. 2017;7(1):14041.
[54] Richely E, Durand S, Melelli A, Kao A, Magueresse A, Dhakal H, et al. Novel Insight into the Intricate Shape of Flax Fibre Lumen. Fibers. 2021;9(4).
[55] Grégoire M, Barthod-Malat B, Labonne L, Evon P, De Luycker E, Ouagne P. Investigation of the potential of hemp fibre straws harvested using a combine machine for the production of technical load-bearing textiles. Industrial Crops and Products. 2020;145.

 doi:10.20944/preprints202305.2090.v1

[56] Melelli A, Jamme F, Legland D, Beaugrand J, Bourmaud A. Microfibril angle of elementary flax fibres investigated with polarised second harmonic generation microscopy. Industrial Crops and Products. 2020;156.
[57] Madsen B, Aslan M, Lilholt H. Fractographic observations of the microstructural characteristics of flax fibre composites. Composites Science and Technology. 2016;123:151-62.
[58] Bos H. The Potential of Flax Fibres as Reinforcement for Composite Materials, thesis: Technische Universiteit Eindhoven; 2004.